ORNL/TM-2020/1754

Intermediate-Term Thermal Aging Effect Evaluation for Grade 92 and 316L at the LWR Relevant Temperature

Lizhen Tan
Xiang (Frank) Chen

September 30, 2020

OAK RIDGE NATIONAL LABORATORY
MANAGED BY UT-BATTELLE FOR THE US DEPARTMENT OF ENERGY

ORNL/TM-2020/1754

Light Water Reactor Sustainability (LWRS) Program
M3LW-20OR0406023

INTERMEDIATE-TERM THERMAL AGING EFFECT EVALUATION FOR GRADE 92 AND 316L AT THE LWR RELEVANT TEMPERATURE

Lizhen Tan & Xiang (Frank) Chen

Date Published: September 30, 2020

Prepared by
OAK RIDGE NATIONAL LABORATORY
Oak Ridge, TN 37831-6283
managed by
UT-BATTELLE, LLC
for the
US DEPARTMENT OF ENERGY
under contract DE-AC05-00OR22725

CONTENTS

LIST OF FIGURES

LIST OF TABLES

ACKNOWLEDGMENTS

This research was sponsored by the U.S. Department of Energy (DOE), Office of Nuclear Energy (NE), under the Light Water Reactor Sustainability (LWRS) Program. The authors are grateful to Tom Geer and Weicheng Zhong of ORNL for optical and scanning electron microscopy imaging and Eric Manneschmidt of ORNL for mechanical testing. Mikhail Sokolov and Maxim Gussev of ORNL are also appreciated for reviewing this report.

ABSTRACT

Life extension of the existing nuclear reactors imposes accumulated damages, such as higher fluences and longer period of corrosion, to structural materials, which would result in significant challenges to the traditional reactor materials such as type 304 and 316 stainless steels. Advanced alloys with superior radiation resistance will increase safety margins, design flexibility, and economics for not only the life extension of the existing fleet but also new builds with advanced reactor designs. The Electric Power Research Institute (EPRI) teamed up with Department of Energy (DOE) on the Advanced Radiation Resistant Materials (ARRM) program, aiming to develop and test degradation resistant alloys from current commercial alloy specifications by 2021 to a new advanced alloy with superior degradation resistance in light water reactor (LWR)-relevant environments by 2024. Based on a comprehensive microstructure and property screening performed in Phase-1 of the ARRM program, a total of five alloys, together with 316L and X-750 as references, were down-selected for Phase-2 neutron irradiation studies. Because thermal aging could exert a synergistic effect on neutron irradiation due to the low neutron damage rate on the order of 10^{-7} displacements per atom per second (dpa/s), Grade 92 (one of the five down-selected alloys) and two heats of 316L were selected in this task to study the effect of aging at 350°C for 12.5–12.7 kh on microstructure and mechanical properties. The aging time is approximately corresponding to 5 dpa neutron irradiation, which can be served as a reference for the 5-dpa-irradiated samples of the alloys to help understand the independent neutron damage influence on microstructure and mechanical properties. Optical microscopy and scanning electron microscopy were used for microstructural characterization. Hardness, tensile, Charpy impact toughness, and fracture toughness in the ductile regime of the aged samples were examined.

The aging of Grade 92 led to the formation of many Laves phase in sizes of ~100–200 nm and resulted in some reduction in hardness and yield/ultimate tensile strength with some increases in uniform and total plastic elongations, which may have helped the enhancement of Charpy impact toughness, e.g., ~4 J increase in upper-shelf energy and 20.5°C reduction in ductile-brittle transition temperature compared with the unaged condition. The fracture toughness of the aged Grade 92 showed decent toughness of ~303 MPa√m (K_{Jq}) with ~87 tearing modulus at 22°C, which reduced to ~241 MPa√m (~20% reduction) with ~75 tearing modulus at 300°C.

The two heats of 316L are differentiated by their amounts of δ-ferrite, i.e., ~1 vol% in heat T1103 and ~4 vol% in heat N5B8. The two heats of 316L were subjected to 15% cold work (CW) as this condition is often used in nuclear reactors to help trapping radiation-induced defects and thus postpone the steady state swelling stage. The aging did not result in any noticeable microstructure changes, except for possible segregations at grain boundaries that need to be further investigated. The aging resulted in slight reduction in hardness of 316L-T1103 and slight increase in hardness of 316L-N5B8, which is consistent with their tensile testing results. The 15%CW might have introduced some inhomogeneity, resulting in large standard deviations in hardness, which were reduced after the aging. The aged 316L followed the same trend as the unaged condition for the strength and elongation results from the tensile testing. Minimum elongations appeared within ~300–600°C, above which the elongations seem to increase. Unlike the negligible or minor changes in microstructure, hardness and tensile results of the two heats of 316L, their fracture toughness showed noticeable difference. The aged 316L-T1103 showed good toughness of ~350 MPa√m with ~80 tearing modulus at 22°C, which reduced to ~271 MPa√m (~23% reduction) with ~83 tearing modulus at 300°C. In contrast, the aged 316L-N5B8 showed lower toughness of ~244 MPa√m with ~53 tearing modulus at 22°C, which reduced to ~180 MPa√m (~26% reduction) with ~31 tearing modulus at 300°C. The preliminary results indicate that the presence of high volume of δ-ferrite would noticeable impair fracture toughness although it may not influence hardness and tensile properties.

1. INTRODUCTION

Nuclear power currently provides a significant fraction of the United States' non-carbon emitting power generation. In future years, nuclear power must continue to generate a significant portion of the nation's electricity to meet the growing electricity demand, clean energy goals, and to ensure energy independence. New reactors will be an essential part of the expansion of nuclear power. However, given limits on new builds imposed by economics and industrial capacity, the extended service of the existing fleets will also be required.

Nuclear reactors present a very harsh environment for components in service. Components within a reactor core must tolerate high temperatures, corrosion, stress, vibration, and an intense neutron field. With the nominal irradiation temperature of ~290°C in light water reactors (LWRs), actual component temperatures range from 270°C to 370°C depending on the relative position of the component within the reactor core and relative amounts of cooling and gamma heating. Degradation of materials in this environment can lead to reduced performance, and in some cases, sudden failure. Extending the service life of a reactor will increase the total neutron fluence to each component and may result in radiation-induced effects not yet observed in LWR conditions, although this form of degradation has been observed in fast reactor conditions. Increases in neutron fluence may exacerbate radiation-induced or -enhanced microstructural and property changes. Comprehensive reviews on radiation effects on the traditional structural materials of LWRs can be found in Ref. [1,2,3].

It is desirable to have advanced alloys that possess greater radiation resistance than the traditional reactor materials, while having satisfactory performance in other primary properties. The use of such advanced alloys in replacing the traditional reactor materials for the extension of the existing fleets and the building of new reactors will bring improved safety margins and economics. To identify and develop advanced radiation resistant materials, Electric Power Research Institute (EPRI) has partnered with Department of Energy (DOE) Light Water Reactor Sustainability (LWRS) Program to conduct an Advanced Radiation Resistant Materials (ARRM) program. The EPRI report of "Critical Issues Report and Roadmap for the Advanced Radiation-Resistant Materials Program" [4] reviewed the current commercial and advanced alloys that are applicable as core structural materials of LWRs and laid out a detailed research plan to meet the goal of the program.

After comprehensive microstructure and property screening in Phase-1 of the ARRM program [5,6,7,8,9,10], a total of five alloys, together with 316L and X-750 as reference alloys, were down-selected for Phase-2 neutron irradiation studies, from which advanced replacement alloys can be developed and recommended for applications in LWR core internals. Thermal annealing is often considered to play a significant role on the neutron irradiation result because of the low damage rate usually on the order of 10^{-7} displacements per atom per second (dpa/s). Therefore, thermal aging of Grade 92 (one of the down-selected five alloys) and two heats of 316L were selected in this task to demonstrate the effect of aging at 350°C for 12.5–12.7 kh on the microstructure and mechanical properties of the two types of alloys. The aging time is approximately corresponding to 5 dpa neutron irradiation, which can be served as a reference for the 5-dpa-irradiated samples of the alloys to help understand the independent neutron damage influence on microstructure and mechanical properties.

2. EXPERIMENTAL

2.1 ALLOYS

Two high-strength alloys 718A (EPRI version of 718) and 725, together with three low-strength alloys 690, 310, and Grade 92, are down-selected for Phase-2 neutron irradiation study. Alloy X-750 and 316L are used as references for the high- and low-strength alloys, respectively. Grade 92 and 316L are selected in this aging study at 350°C. The compositions in weight percent (wt%) of the steels are listed in Table 1, together with the fabrication methods and specific heat treatments for the steels listed in Table 2. Two heats of 316L are included in the aging study, which are primarily differentiated by their δ-ferrite amounts. Following the ASTM A800/A800M-20, "Standard practice for estimating ferrite content of stainless steel castings containing both ferrite and austenite", the ratio of Cr_e/Ni_e = (Cr + 1.5Si + 1.4Mo – 4.99)/(Ni + 30C + 0.5Mn + 26(N – 0.02) + 2.77) gives 0.929 for heat T1103 and 1.017 for heat N5B8, corresponding to δ-ferrite amount of 0–3.5 vol% and 1.5–7 vol%, respectively. Therefore, we can roughly estimate ~1 vol% δ-ferrite in heat T1103 while ~4 vol% δ-ferrite in heat N5B8. The application of 316L in LWRs is often in the state of 15–20% cold work (CW) to increase irradiation defects trapping sites and thus postpone the occurrence of steady state swelling. Accordingly, 15% CW was applied to the two heats of 316L.

Table 1. Vendor reported compositions (wt%) of Grade 92 and 316L with Fe as balance

Alloy	Heat	Cr	Ni	Mo	W	V	Nb	Si	Mn	C	N	P	S	Cu
Grade 92	011448	8.81	0.12	0.36	1.78	0.18	0.08	0.1	0.4	0.091	0.046	<0.005	<0.0005	<0.01
316L	T1103	17.5	12.3	2.3	-	-	-	0.46	1.8	0.022	0.06	0.027	0.001	0.2
316L	N5B8	16.66	10.01	2.00	-	-	-	0.31	1.43	0.014	0.05	0.032	0.0013	0.41

Table 2. Fabrication condition of Grade 92 and 316L

Alloy	Heat number	Fabrication method [a]	Heat treatment [b]
Grade 92	011448	VIM	1130°C/0.5h/WQ + 600°C/1h/AC + 750°C/4h/AC
316L	T1103	EAM	1050°C/0.5h/WQ
316L	N5B8	EAF, AOD, Continuous casting	>1038°C/WQ

[a] VIM – vacuum induction melting; EAM – electric arc melting; EAF – electric arc furnace; AOD – argon oxygen decarburization

[b] AC – air cooling; WQ – water quenching

2.2 THERMAL AGING

Blocks of materials from the heats of Grade 92 and 316L were aged in box furnace at 350°C for 12.7 kh for Grade 92 and 12.5 kh for 316L.

2.3 MICROSTRUCTURAL CHARACTERIZATION

Metallographic samples were prepared from the aged blocks of the materials, which were grinded and polished to a mirror finish. The Glyceregia etchant was used for 316L. Optical micrograph were taken from the etched 316L samples. Grade 92 was characterized by scanning electron microscopy in the secondary electron image (SEI) and backscattered electron image (BEI) modes.

2.4 MICROHARDNESS TEST

Vickers microhardness were measured on the metallographic samples using 1,000 kgf load with 20 s dwelling time. Five measurements were conducted for each sample to obtain statistical hardness results.

2.5 TENSILE TEST

Type SS-3 miniature specimens were machined from the aged blocks of the materials with the gauge length direction parallel to the rolling direction of plates. Figure 1 shows the geometry of type SS-3 specimens. Tensile tests were conducted in air at temperatures from room temperature up to 700°C, following the ASTM E8 "Standard test methods for tension testing of metallic materials" and E21 "Standard test methods for elevated temperature tension tests of metallic materials". Tests were performed using an MTS tensile testing system with a load cell possessing 22 kN (5000 lbf) capacity, which is integrated in the load train and placed in the water-cooled zone below the hot zone of the furnace. Tensile testing was performed at a crosshead speed of 0.018 in/min to achieve the nominal strain rate of 0.001 s^{-1}. The tensile testing system, load cells, and the temperature controller have been routinely calibrated.

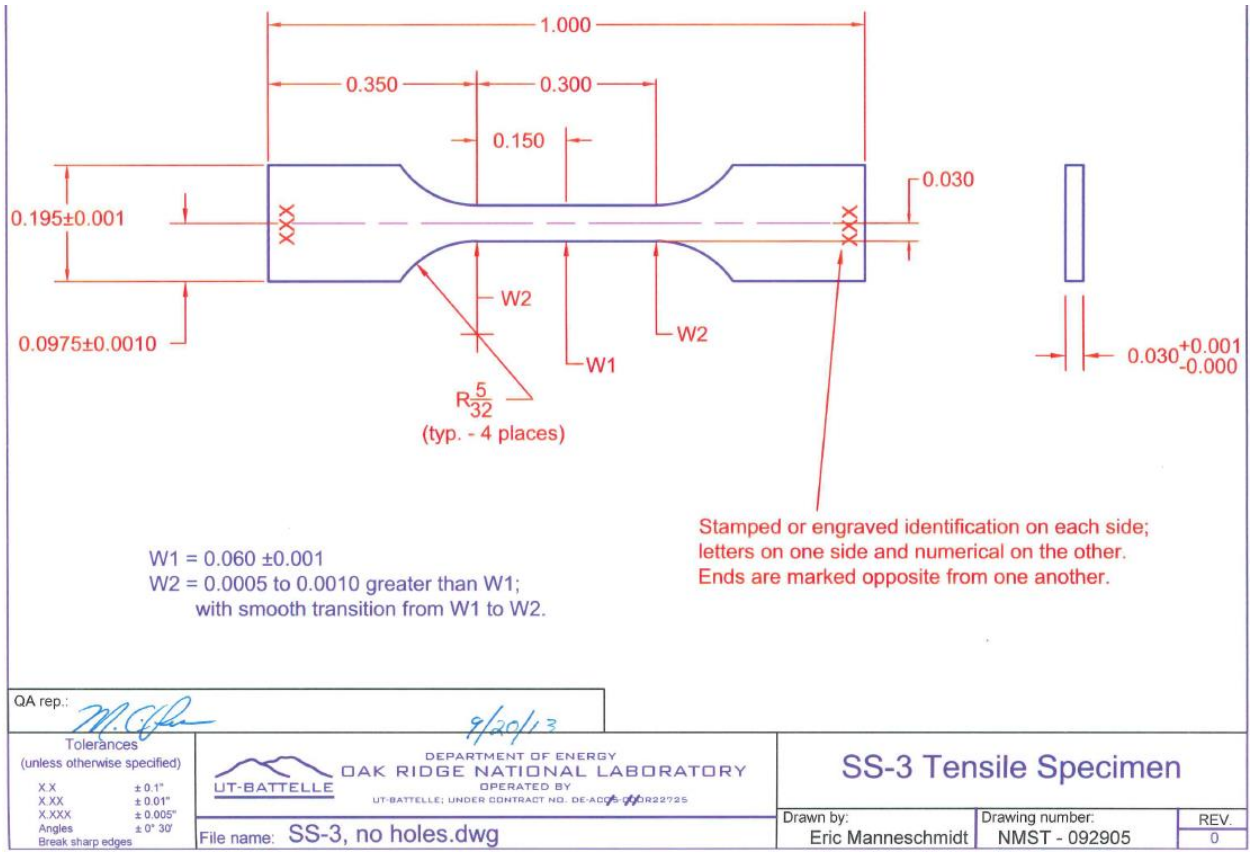

Figure 1. Geometry of type SS-3 miniature specimen in inch.

2.6 CHARPY V-NOTCH IMPACT TEST

Half-size Charpy V-notch specimens, with its geometry shown in Figure 2, were machined from the aged block of Grade 92 with the ligament under the V-notch in parallel with the longitudinal direction of the plates, i.e., the T-L (transverse-longitudinal) orientation. Charpy impact tests were conducted on a Tinius Olsen Charpy 300 ft-lb machine according to the ASTM E23-12c, "Standard test methods for notched bar impact testing of metallic materials." The measurement calibration of the Charpy machine is performed annually through testing of specimens with certified values to verify the accuracy of the machine. The certified specimens are obtained from the National Institute of Standards and Technology (NIST). The half-size Charpy V-notch specimens were tested at temperatures ranging from –150°C to 100°C to measure the absorbed impact energies, i.e., upper-shelf energy (USE), and to determine ductile-brittle transition temperature (DBTT) of the aged Grade 92.

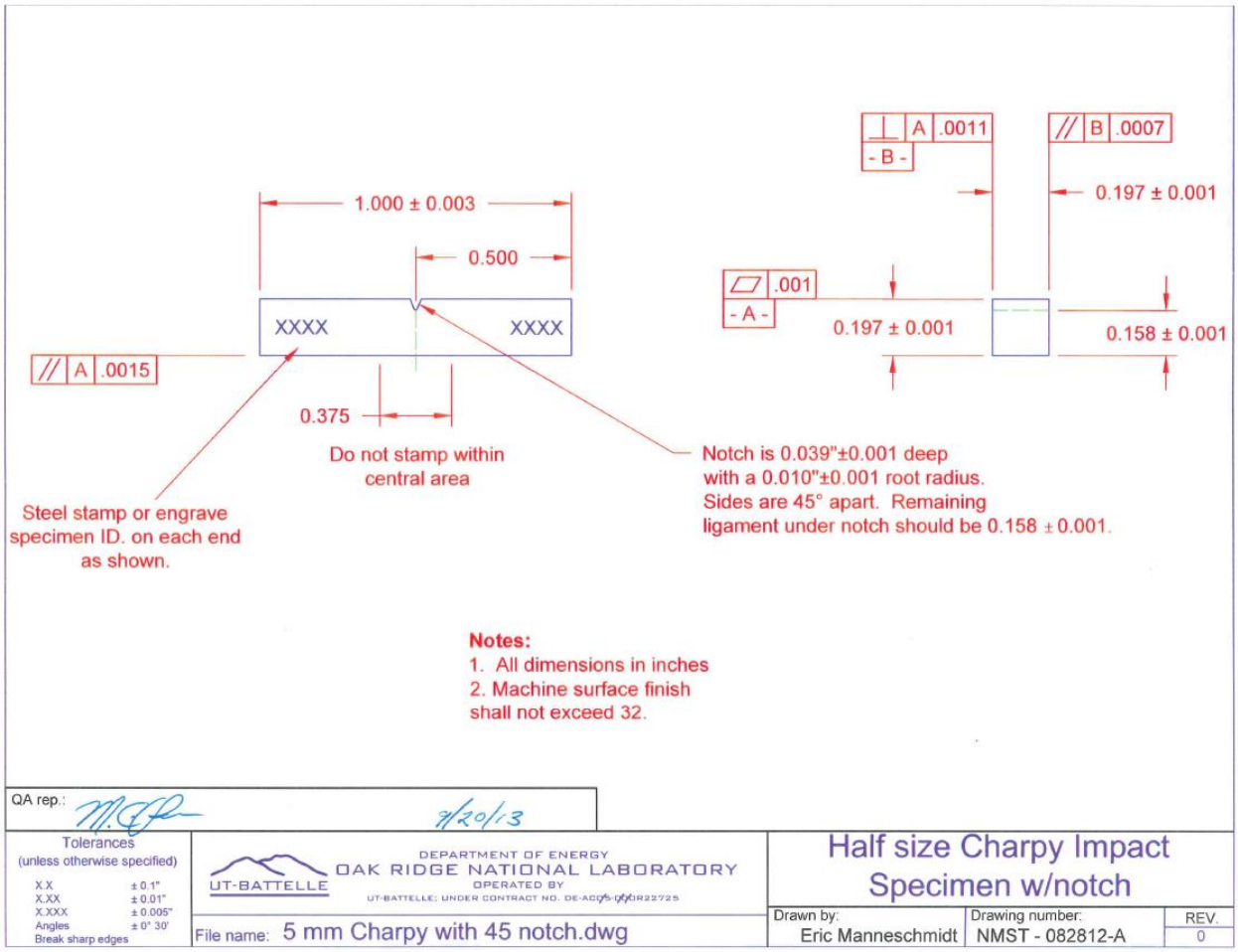

Figure 2. Geometry of half-size Charpy V-notch specimen in inch.

2.7 FRACTURE TOUGHNESS TEST

Compact tension specimens according to the specifications in Figure 3 for 0.2T and Figure 4 for 0.25T were extracted along the T-L orientation from the aged plates of Grade 92 and 316L, respectively. A total of four specimens per material were tested with a computer-controlled test and data acquisition system in accordance with the ASTM E1820, "Standard Test Method for Measurement of Fracture Toughness", for

the ductile regime at 22°C and 300°C. The specimens were fatigue pre-cracked to the crack length to specimen width (a/W) ratio of about 0.5 and then side-grooved (10% thickness from each side surface was removed) before fracture testing. Specimens were tested in the laboratory on a 98-kN (22-kip) capacity servo-hydraulic machine. All tests were conducted with a quasi-static loading rate, with an outboard clip gage having a central flexural beam that was instrumented with four strain gages in a full-bridge configuration. An automated normalization analysis software was used to derive and analyze the J-integral and crack extension curves (J-R curves) [11].

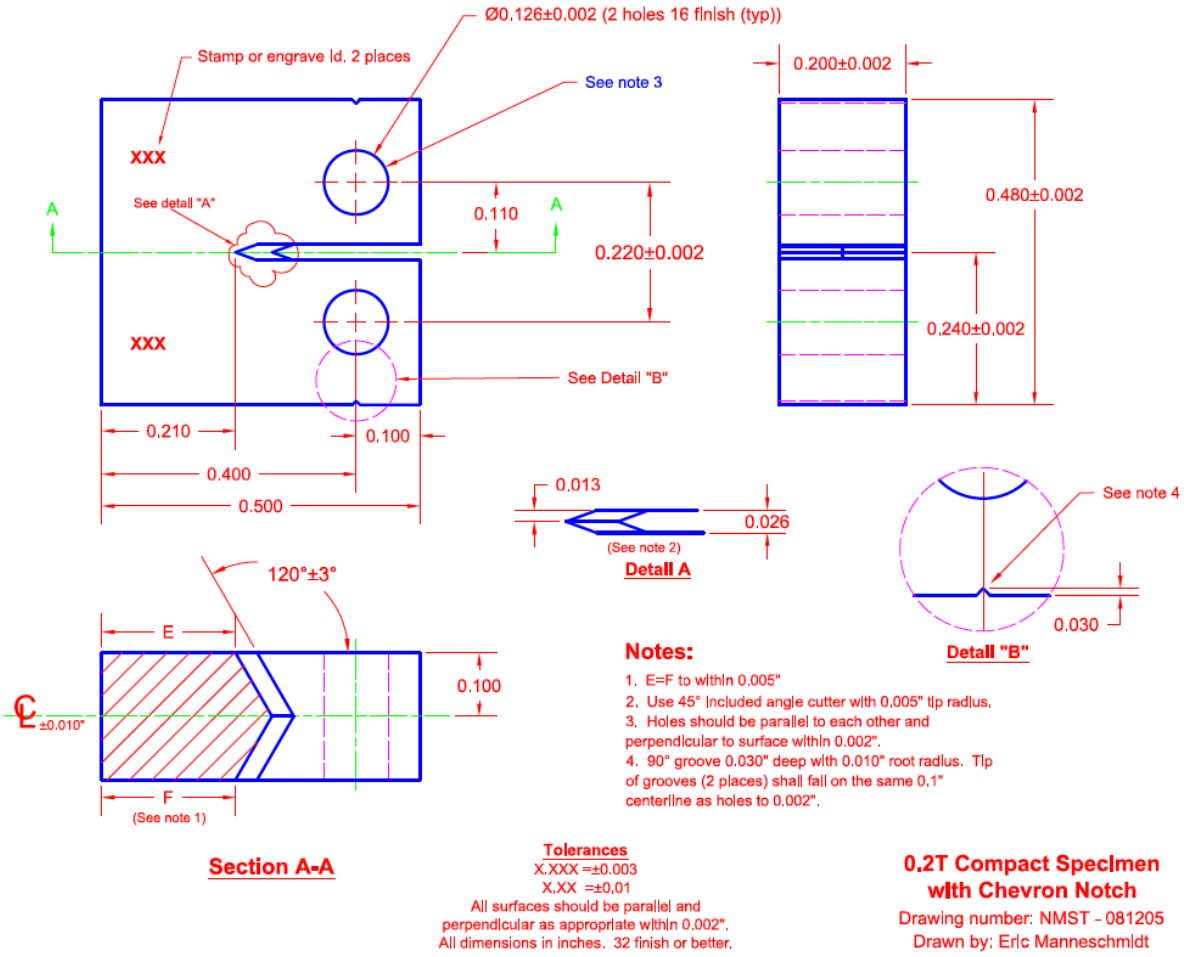

Figure 3. Specification of 0.2T compact tension specimen (dimensions are in inches).

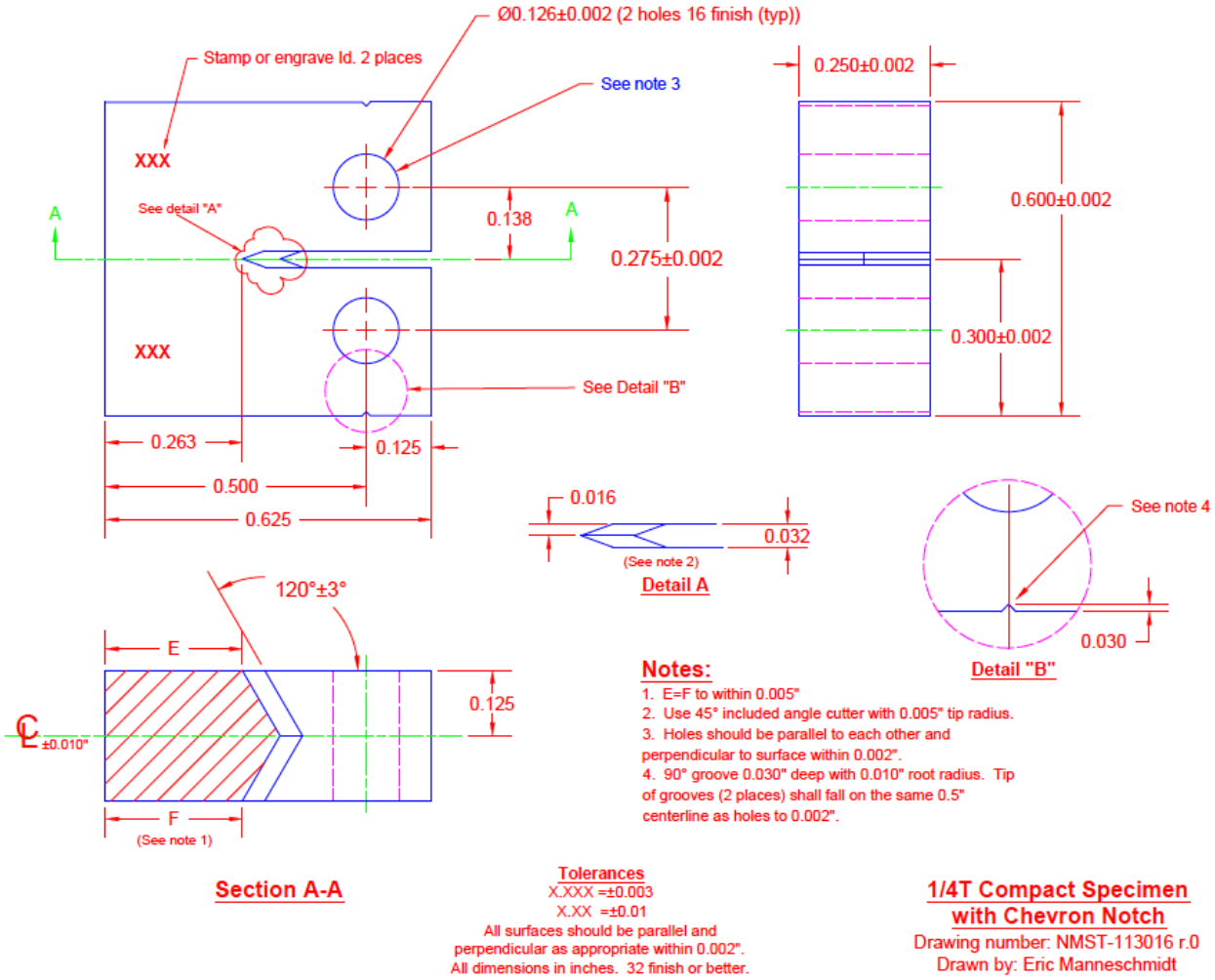

Figure 4. Specification of 0.25T compact tension specimen (dimensions are in inches).

3. AGING-INDUCED MICROSTRUCTURAL EVOLUTION

3.1 Grade 92 (Ht. 011448)

The microstructures of Grade 92 aged at 350°C for 12.7 kh are shown in Figure 5 from two locations (in two rows), with the left column in SEIs and the right column in BEIs. The aging did not result in noticeable grain and lath structure changes to Grade 92. The BEIs show many small white precipitates primarily in ~100–200 nm, which primarily decorate the block/packet/prior-austenite boundaries. The small white precipitates are rich in W with a high–Z to yield a high contrast under the BEIs, which are believed to be Laves phase, e.g., Fe_2W. A few coarse white precipitates in ~400 nm, e.g., the one in Fig. 5b pointed by a white arrow, which are rich in Nb and believed to be MX (M=Nb, X=C/N) precipitates. A few black features in both SEIs and BEIs, with sizes as large as ~500 nm as exemplified in Fig. 5d pointed by a white arrow, were also observed in the material, which are believed to be inclusions of the material. Comparing the (c) SEI with (d) BEI, we can see many fine precipitates (<~100 nm) in dark grey distributed on lath boundaries and in the matrix on the right side of the SEI, which are not seeable in the corresponding BEI. The dark grey precipitates are believed to be $M_{23}C_6$ (M=Cr-rich) and MX (M=V, X=C/N) precipitates. Among the microstructure features, only the Laves phase was induced by the aging.

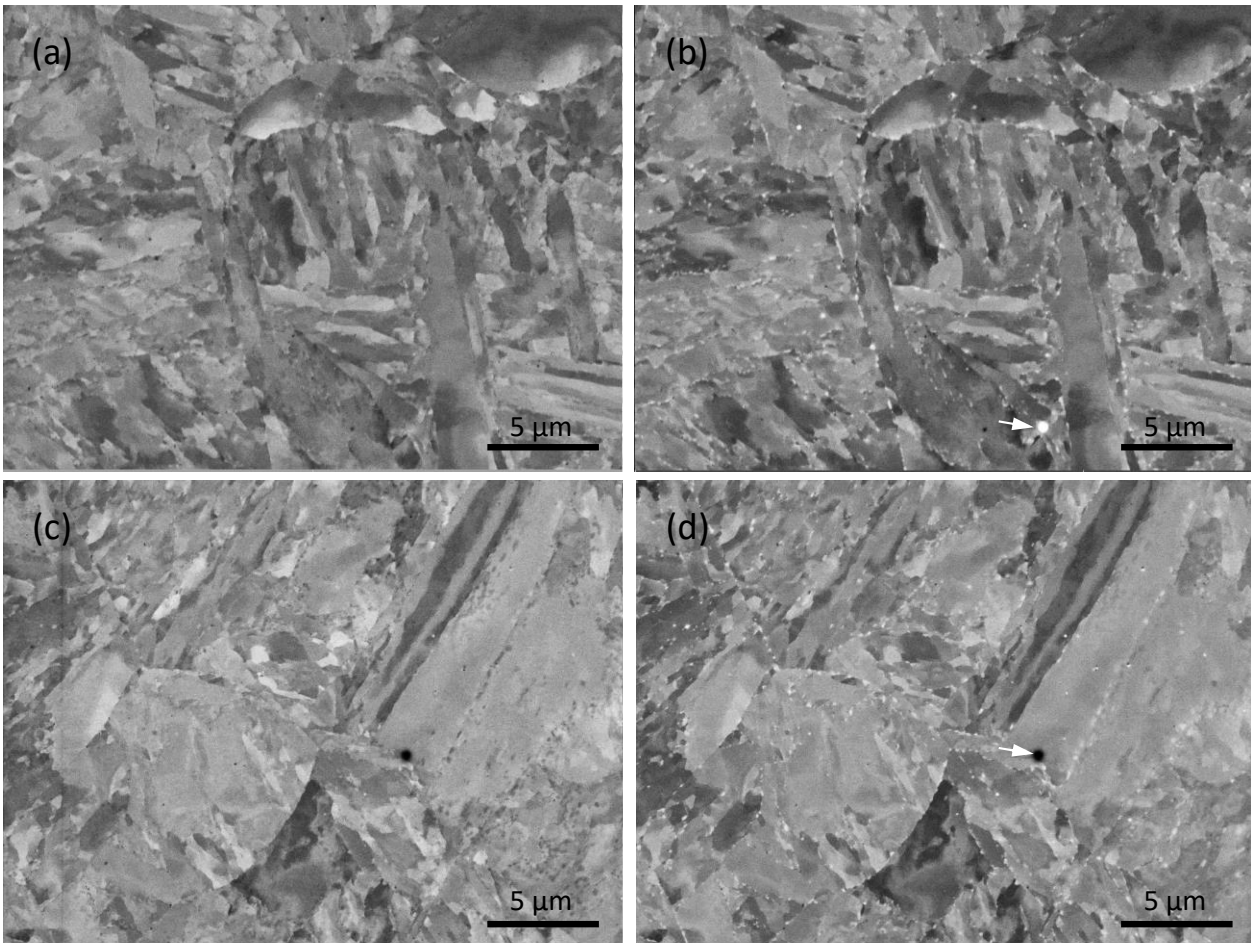

Figure 5. (a,c) Secondary electron images and (b,d) corresponding backscattered electron images of Grade 92 aged at 350°C for 12.7 kh.

3.2 316L (Ht. T1103)

Figure 6 compares the optical micrographs of the 15%CW 316L heat T1103 (~1 vol% δ-ferrite) prior to aging with that aged at 350°C for 12.5 kh. A few short strings of δ-ferrite, e.g., those pointed by black arrows in Fig. 6a, are seeable at some of the austenite grain boundaries in the 15%CW 316L prior to aging. The higher magnification micrograph in Fig. 6b indicates the presence of twins and some slip lines induced by the 15%CW. After the aging, the grain structure with the presence of short strings, twins and slip lines were not noticeably changed. However, the high magnification micrograph in Fig. 6d seems to have increased contrast at some of the boundaries, which may indicate segregation and need to be further investigated.

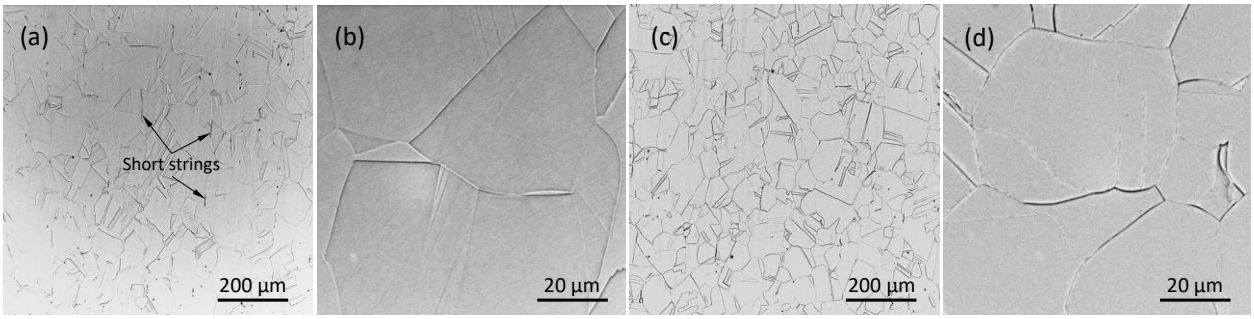

Figure 6. Optical micrographs of 15%CW 316L (T1103): (a,b) prior to aging and (c-d) aged at 350°C for 12.5 kh.

3.3 316L (Ht. N5B8)

Figure 7 compares the optical micrographs of the 15%CW 316L heat N5B8 (~4 vol% δ-ferrite) prior to aging with that aged at 350°C for 12.5 kh. Two type of δ-ferrite, i.e., Widmanstätten and short strings pointed by black arrows in Fig. 7a, were observed in this heat of 316L prior to aging. The high magnification micrograph in Fig. 7b shows some slip lines induced by the 15%CW. It is not clear whether the small black features in Fig. 7b are inclusions or precipitates because of the etched surface. After the aging, the grain structure with the presence of two types of δ-ferrite and slip lines were not noticeably changed. However, many long strings of δ-ferrite are seeable from Fig. 7c, which is not induced by the aging but indicates the inhomogeneous distribution of long and short strings of δ-ferrite in the heat of 316L. The high magnification micrograph in Fig. 7d shows many slip lines from the 15%CW and the two types of δ-ferrite at boundaries.

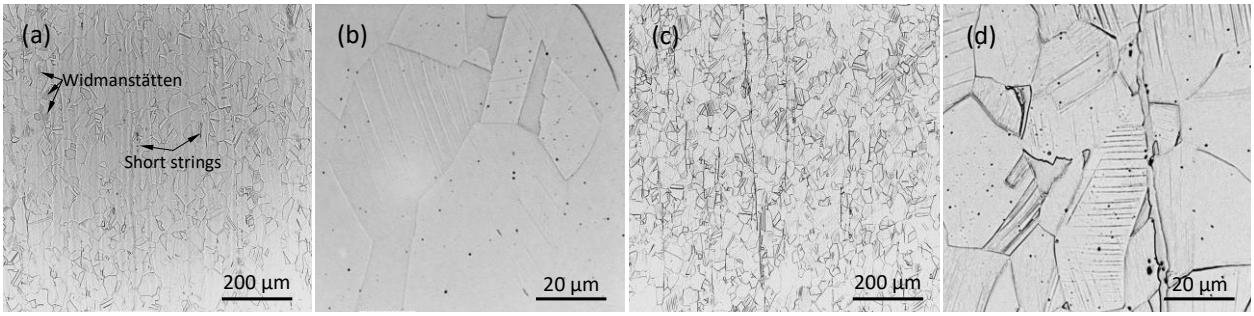

Figure 7. Optical micrographs of 15%CW 316L (N5B8): (a,b) prior to aging and (c-d) aged at 350°C for 12.5 kh.

4. AGING-INDUCED CHANGES IN MECHANICAL PROPERTIES

4.1 MICROHARDNESS

The Vickers hardness results of Grade 92 (011448), 316L (T1103), and 316L (N5B8) in the conditions of prior to aging and after the aging at 350°C for 12.5–12.7 kh are shown in Figure 8. The 15%CW applied to 316L resulted in large standard deviations, which are reduced after aging, indicating the aging led to some local stress relaxation. The aging slightly reduced the hardness of Grade 92 and 316L (T1103), but slightly increased the hardness of 316L (N5B8).

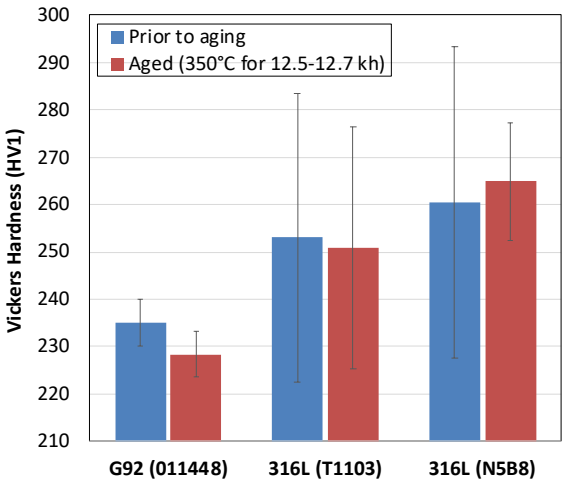

Figure 8. Vickers hardness results comparison of Grade 92 (#011448), 316L (#T1103), and 316L (#N5B8) between the prior to aging and aged at 350°C for 12.7 kh (G92) and 12.5 kh (316L).

4.2 TENSILE PROPERTIES

The stress-strain curves of the tensile-tested samples of Grade 92 and two heats of 316L are shown in Figure 9. The left column is the results prior to aging and the right column is the results after the aging at 350°C for 12.5–12.7 kh. The test temperatures for Grade 92 prior to aging (Fig. 9a) are different from the other steels and conditions because the temperatures of the furnace were calibrated after the testing, while the temperatures of the furnace were calibrated before the testing of Grade 92 after aging and the 316L samples. The general changes after aging for Grade 92 and the two heats of 316L are not dramatic compared with the prior to aging condition. The detailed temperature-dependent changes in yield strength, ultimate tensile strength, uniform plastic elongation, and total plastic elongation are shown in Figure 10.

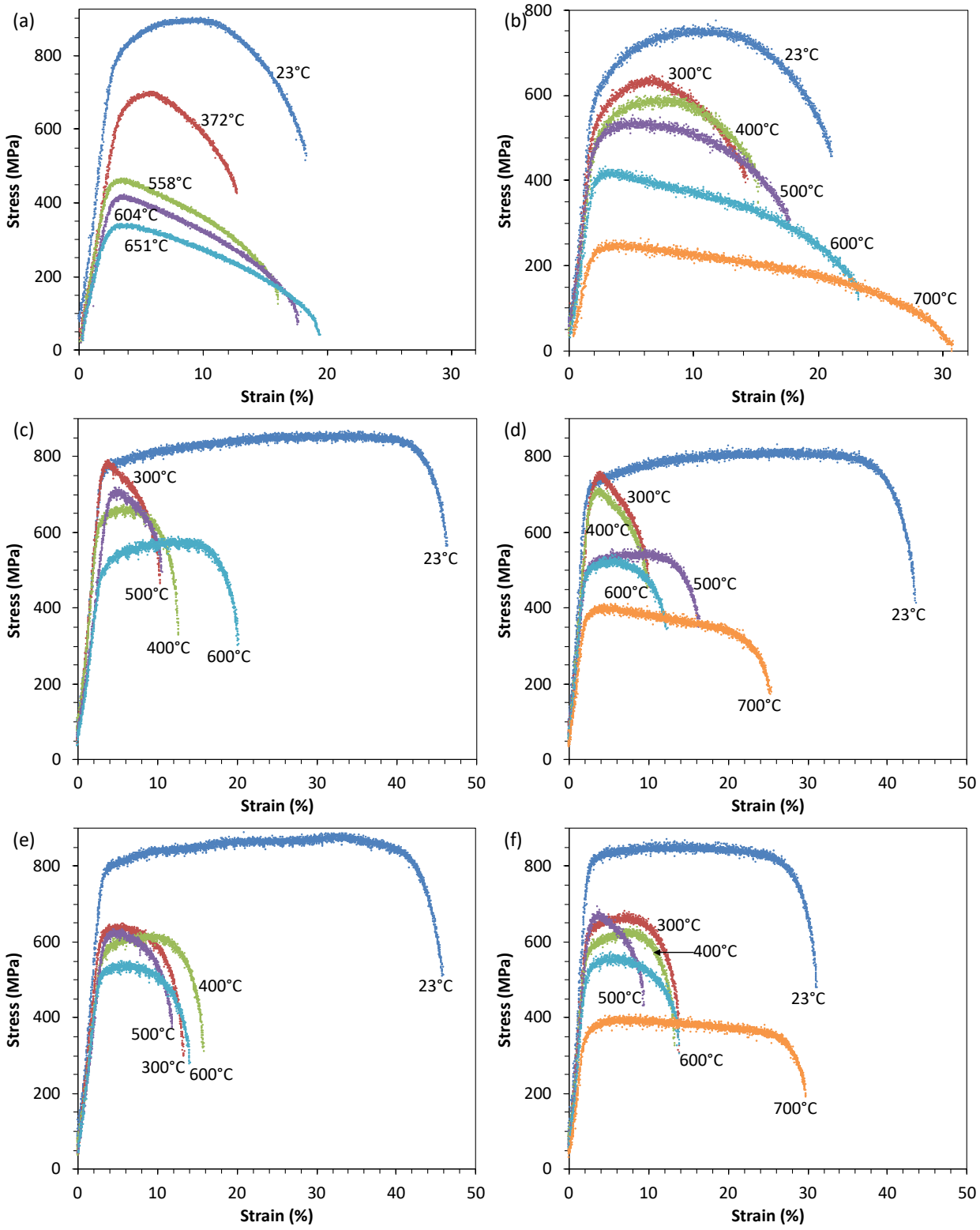

Figure 9. Tensile curves of (a) Grade 92 in the initial N&T condition, (b) Grade 92 aged at 350°C for 12.7 kh, (c) 15%CW 316L (T1103), (d) 15%CW 316L (T1103) aged at 350°C for 12.5 kh, (e) 15%CW 316L (N5B8), and (f) 15%CW 316L (N5B8) aged at 350°C for 12.5 kh.

The temperature-dependent yield strength of Grade 92 and the two heats of 316L is shown in Figure 10a. The aged Grade 92 showed ~170 MPa yield strength reduction at room temperature. The yield strength reduction reduced with the increasing temperature to be comparable with the unaged condition at ~550–600°C, above which the aged Grade 92 seems to have a higher yield strength than the unaged condition. Unlike Grade 92, the yield strength evolution of 316L was not monotonic decreasing with the increasing temperature, which is likely attributable to inhomogeneous microstructure or internal stresses induced by the 15%CW. The aged 316L generally followed the same temperature-dependent yield strength change as the unaged condition. The 316L-T1103 showed slight (~60 MPa) reductions in yield strength, while the 316L-N5B8 showed slight (~20 MPa) increases in yield strength. The temperature-dependent ultimate tensile strength changes of Grade 92 and the two heats of 316L as shown in Figure 10b followed the same trend as the yield strength in Figure 10a, except for different magnitudes in the changes.

With the aging-induced softening in Grade 92, the uniform plastic elongation and total plastic elongation of the aged Grade 92 slightly increased at the testing temperatures as shown in Figure 10c-d. In contrast, the uniform and total plastic elongations of 316L showed different levels of reductions, e.g., ~5% reduction in uniform plastic elongation for 316L-T1103 while ~17% reduction for 316L-N5B8 at room temperature as shown in Figure 10c-d. The uniform and total plastic elongations of the two heats of 316L reached minimum values at ~300–600°C, above which their elongations seem to be increased.

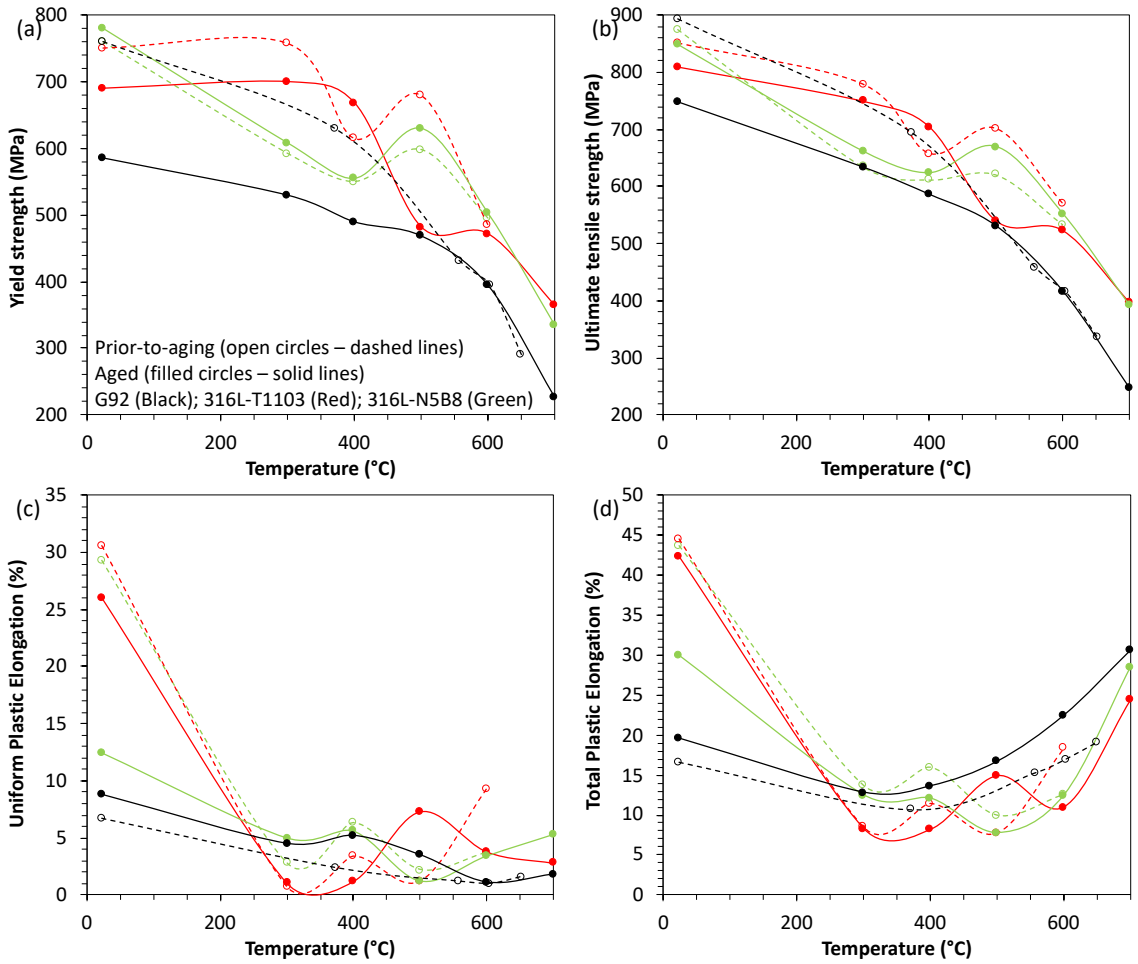

Figure 10. Temperature-dependent (a) yield strength, (b) ultimate tensile strength, (c) uniform plastic elongation, and (d) total plastic elongation of the 350°C-aged Grade 92 and 316L compared with the unaged condition.

4.3 CHARPY IMPACT TOUGHNESS

The Charpy impact test results of the aged Grade 92 specimens compared with the unaged results are shown in Figure 11. To obtain DBTT and USE, an impact energy-temperature curve was generated by fitting the data with a hyperbolic tangent function $E = a + b \tanh[(T - T_0)/c]$, where T is test temperature and a, b, c and T_0 are regression coefficients. In this study, T_0 is the mathematical DBTT, corresponding to the mean value of USE and lower-shelf energy (LSE), i.e., 1/2USE assuming LSE = 0 in this study. Figure 11 shows that the aged Grade 92 has generally higher absorbed impact energies than the unaged condition, which lead to a higher USE by ~4 J and a lower DBTT by 20.5°C for the aged Grade 92 compared with the unaged condition. The improved impact toughness of the aged Grade 92 is likely benefited from the reduced yield strength with increased elongations as shown in Figure 10. The aging-induced Laves phase as shown in Figure 5 did not impair the impact toughness of the aged specimens.

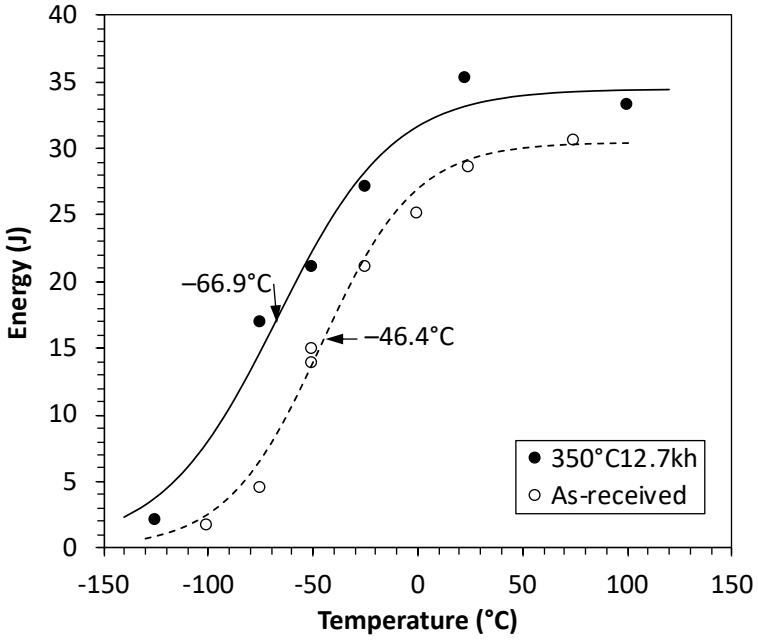

Figure 11. Temperature-dependent absorbed energies of the as-received and aged (350°C for 12.7 kh) Grade 92 specimens.

4.4 FRACTURE TOUGHNESS

The J-R curves are shown in Figure 12 for Grade 92, 316L-T1103, and 316L-N5B8 after thermal aging at 350°C for 12.5–12.7 kh with fracture toughness results summarized in Table 3. All three materials exhibited a similar effect of the temperature on fracture toughness (K_{Jq}) and tearing modulus. At the same temperature (22°C or 300°C), small scattering was observed within one material for fracture toughness and tearing modulus, which is normal for the type of testing. Comparing results at 22°C, elevated temperature at 300°C led to much lower toughness values and slight lower tearing modulus values. The fracture toughness of the aged Grade 92 showed decent toughness of ~303 MPa$\sqrt{m}$ (K_{Jq}) with ~87 tearing modulus at 22°C, which reduced to ~241 MPa$\sqrt{m}$ (~20% reduction) with ~75 tearing modulus at 300°C. Comparing two different heats of aged 316L, 316L-T1103 with ~1 vol% δ-ferrite exhibited much higher toughness and tearing modulus values than 316L-N5B8 with ~4 vol% δ-ferrite.

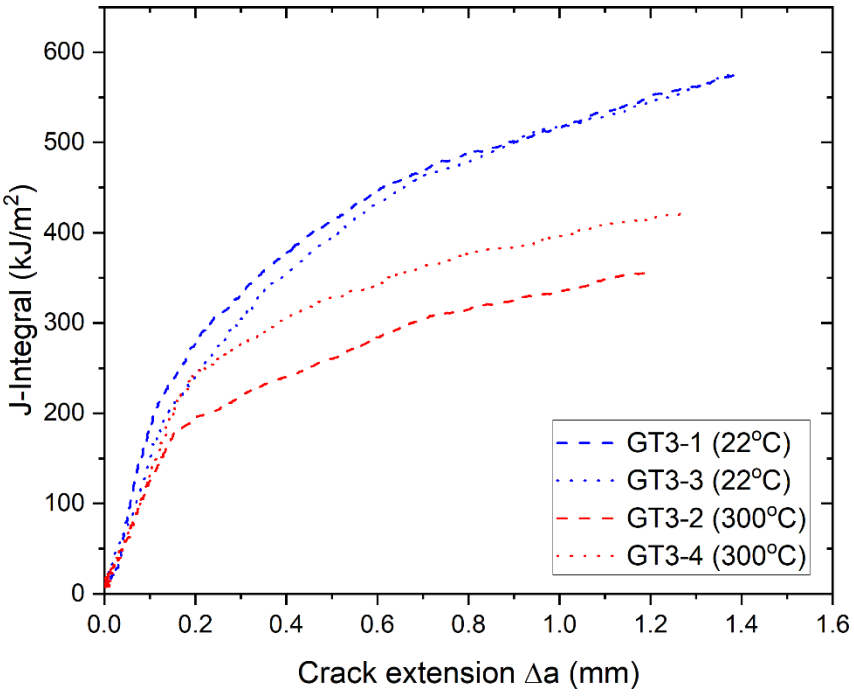
J-Integral (kJ/m^2)
Crack extension Δa (mm)
GT3-1 (22°C)
GT3-3 (22°C)
GT3-2 (300°C)
GT3-4 (300°C)

(a)

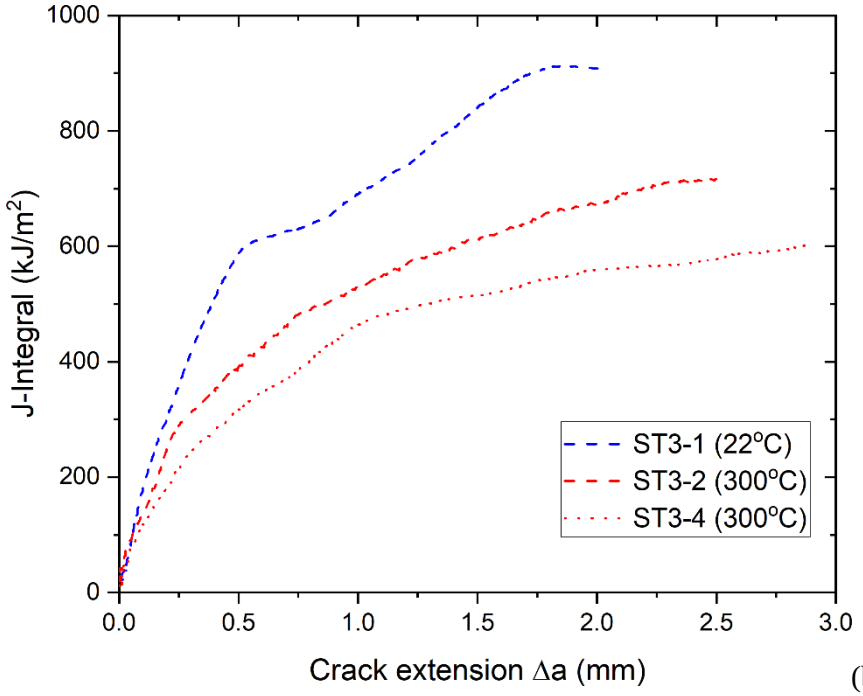
J-Integral (kJ/m^2)
Crack extension Δa (mm)
ST3-1 (22°C)
ST3-2 (300°C)
ST3-4 (300°C)

(b)

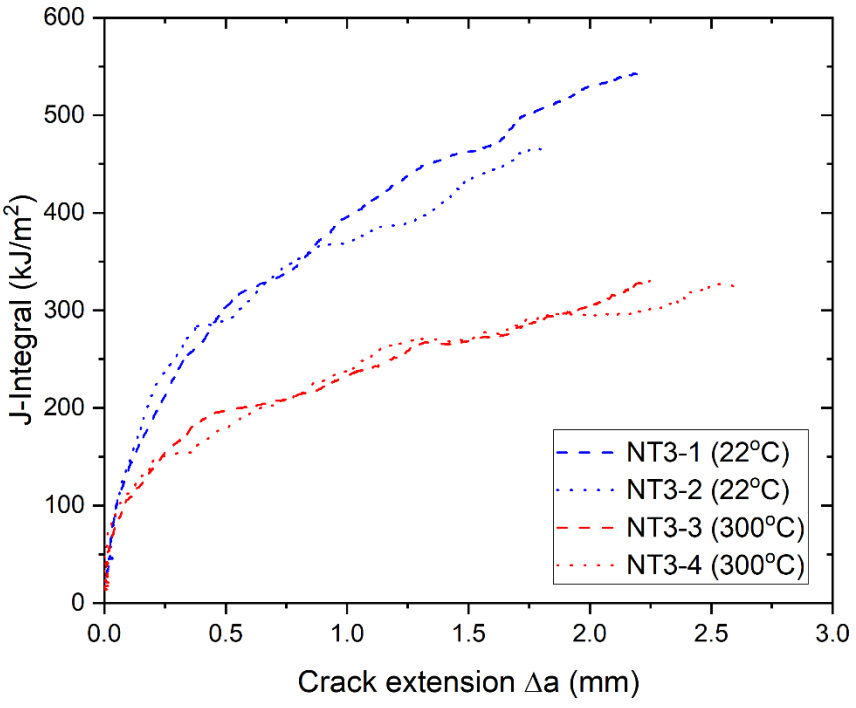

(c)

Figure 12. Room temperature and 300°C J-R curve fracture toughness results of Grade 92 in (a), 316L-T1103 in (b), and 316L-N5B8 in (c) after thermal aging at 350°C for 12.5–12.7 kh.

Table 3. Summary of fracture toughness test results for Grade 92, 316L-T1103, and 316L-N5B8 aged at 350°C for 12.5–12.7 kh

Alloy	Specimen ID	Test temperature (°C)	Toughness K_{Jq} (MPa√m)	Avg. toughness (MPa√m)	Tearing modulus	Avg. tearing modulus
Grade 92	GT3-1	22	306.6	302.9	81.3	87.2
	GT3-3	22	299.1		93.1	
	GT3-2	300	223.9	240.6	80.2	74.8
	GT3-4	300	257.2		69.3	
316L-T1103	ST3-1	22	349.9	349.9	79.8	79.8
	ST3-2	300	289.1	270.9	84.7	83.1
	ST3-4	300	252.7		81.5	
316L-N5B8	NT3-1	22	241.7	243.6	59.9	53.3
	NT3-2	22	245.6		46.8	
	NT3-3	300	184.7	180.0	29.0	30.9
	NT3-4	300	175.4		32.9	

5. SUMMARY

Blocks of Grade 92 and two heats of 316L (T1103 and N5B8) were aged at 350°C for 12.7 and 12.5 kh, respectively. Metallographic samples, type SS-3 tensile specimens along the longitudinal direction, half-size Charpy V-notch specimens in the T-L orientation, and 0.2T or 0.25T compact tension fracture toughness specimens in the T-L orientation were machined from the aged blocks of materials for the respective microstructural characterization and mechanical property evaluation.

The aging of Grade 92 led to the formation of many Laves phase in sizes of ~100–200 nm and resulted in some reduction in hardness and yield/ultimate tensile strength with some increases in uniform and total plastic elongations, which may have helped the enhancement of Charpy impact toughness, e.g., ~4 J increase in upper-shelf energy and 20.5°C reduction in ductile-brittle transition temperature compared with the unaged condition. The fracture toughness of the aged Grade 92 showed decent toughness of ~303 MPa√m (K_{Jq}) with ~87 tearing modulus at 22°C, which reduced to ~241 MPa√m (~20% reduction) with ~75 tearing modulus at 300°C.

The two heats of 316L are differentiated by their amounts of δ-ferrite, i.e., ~1 vol% in heat T1103 and ~4 vol% in heat N5B8. The two heats of 316L were subjected to 15% cold work (CW) as this condition is often used in nuclear reactors to help trapping radiation-induced defects and thus postpone the steady state swelling stage. The aging did not result in any noticeable microstructure changes, except for possible segregations at grain boundaries that need to be further investigated. The aging resulted in slight reduction in hardness of 316L-T1103 and slight increase in hardness of 316L-N5B8, which is consistent with their tensile testing results. The 15%CW might have introduced some inhomogeneity, resulting in large standard deviations in hardness, which were reduced after the aging. The aged 316L followed the same trend as the unaged condition for the strength and elongation results from the tensile testing. Minimum elongations appeared within ~300–600°C, above which the elongations seem to increase. Unlike the negligible or minor changes in microstructure, hardness and tensile results of the two heats of 316L, their fracture toughness showed noticeable differences. The aged 316L-T1103 showed good toughness of ~350 MPa√m with ~80 tearing modulus at 22°C, which reduced to ~271 MPa√m (~23% reduction) with ~83 tearing modulus at 300°C. In contrast, the aged 316L-N5B8 showed lower toughness of ~244 MPa√m with ~53 tearing modulus at 22°C, which reduced to ~180 MPa√m (~26% reduction) with ~31 tearing modulus at 300°C. The preliminary results indicate that the presence of high volume of δ-ferrite would noticeable impair fracture toughness although it may not influence hardness and tensile properties.

REFERENCES

[1] E.A. Kenik, J.T. Busby, Radiation-induced degradation of stainless steel light water reactor internals, Mater. Sci. Eng. R 73 (2012) 67–83.

[2] F.A. Garner, Radiation damage in austenitic steels, in: R.J.M. Konings, T.R. Allen, R.E. Stoller, S. Yamanaka, Comprehensive Nuclear Materials, Elsevier, The Netherlands, 2012.

[3] L. Tan, R.E. Stoller, K.G. Field, Y. Yang, H. Nam, D. Morgan, B.D. Wirth, M.N. Gussev, J.T. Busby, Microstructural evolution of type 304 and 316 stainless steels under neutron irradiation at LWR relevant conditions, JOM 68 (2016) 517–529.

[4] Critical Issues Report and Roadmap for the Advanced Radiation-Resistant Materials Program, EPRI, Palo Alto, CA and the U.S. Department of Energy, Washington, DC: 2012. 1026482.

[5] L. Tan, D.T. Hoelzer, J.T. Busby, Microstructure and basic mechanical properties of the procured advanced alloys for the advanced radiation resistant materials program, ORNL/TM-2014/439, September 22, 2014.

[6] L. Tan, B.A. Pint, High-temperature steam oxidation testing of select advanced replacement alloys for potential core internals, ORNL/TM-2017/228, May 19, 2017.

[7] X. Chen, L. Tan, Fracture toughness evaluation of select advanced replacement alloys for LWR core internals, ORNL/TM-2017/377, August 25, 2017.

[8] L. Tan, B.A. Pint, X. Chen, Toughness and high-temperature steam oxidation evaluations of advanced alloys for core internals, ORNL/TM-2016/371, September 16, 2016.

[9] L. Tan, T. Chen, B.A. Pint, Steam oxidation behavior of Ni-base superalloys 690, 725 and X-750 at 600 and 650°C, Corrosion Science 157 (2019) 487–497.

[10] D.W. Sandusky, M. Morra, J.L. Nelson, Guidelines for material procurements for use in light water reactor environments, 2015 Technical Report 3002005623, Electric Power Research Institute, September 2015.

[11] A. Esteban Linares, L. Clowers, X. Chen, M. Sokolov, and R. Nanstad, Using Automated J-R Curve Analysis Software to Simplify Testing and Save Time, Advanced Materials & Processes, Vol. 177, No. 2, February/March 2019